

# Seismic Network Calibration for Retrieving Accurate Moment Tensors

by Rosalia Davi and Václav Vavryčuk

**Abstract** We present a method for calibrating seismic networks in order to retrieve highly accurate seismic moment tensors. The method is based on a joint inversion of large datasets of earthquakes for moment tensors and for amplifications of the network stations, which encompass the instrumental amplifications of sensors and the gain factor of the acquisition system, as well as the local site effects neglected in modeling of Green's functions. The method is capable of detecting the reverse polarity of sensors, incorrect orientation of sensors, or anomalous site effects caused by local geological conditions at individual stations. The robustness and accuracy of the method are tested on synthetic data with different noise levels, station configurations, and a variety of focal mechanisms. The numerical modeling confirms that the inversion code works well and yields robust results. The tests show that the moment tensors, calculated from data of properly calibrated seismic networks, are significantly more accurate. Finally, the method is applied to observations in West Bohemia, Czech Republic, in order to calibrate a network of 22 local seismic stations operated in this region and to calculate accurately the double-couple (DC) and non-double-couple (non-DC) components of moment tensors of 200 selected micro-earthquakes. The results indicate that the method is efficient and can easily be used to calibrate other networks. For example, it can be used in inverting laboratory data, where the coupling effects between the sensor and a rock sample are difficult to quantify, or mining and borehole data, where the calibration and orientation of the sensors are frequently unknown. Moreover, the method can be applied to all studies, which deal with retrieving and interpreting highly accurate moment tensors and their DC and non-DC components.

## Introduction

Moment-tensor inversion is one of the most common tools used for studying earthquakes, finding applications for a large variety of datasets from micro- to macro-scales (Dziewonski *et al.*, 1981; Sipkin, 1986; Lay and Wallace, 1995; Julian *et al.*, 1997; Trifu and Shumila, 2000; Šílený and Hofstetter, 2002; Vavryčuk, 2002, 2007; Cesca *et al.*, 2006; Zahradník *et al.*, 2008a,b; Davi *et al.*, 2010; De Barros *et al.*, 2011). Moment-tensor inversion is a powerful but data-demanding procedure that requires a good velocity model, an accurate hypocenter location, and high-quality data with a high signal-to-noise ratio, recorded by many stations with good azimuthal coverage (Ford *et al.*, 2010). However, the quality of data cannot always be considered optimum as various problems related to the functioning of stations are common. The sensors may be incorrectly calibrated or may have reversed polarity; the horizontal components of the stations may be misoriented, or amplification factors may change in time. Additionally, in laboratory-based acoustic emission experiments, reliable calibration is, in general, difficult to ensure because of the coupling effects between the sensor and the specimen. In boreholes or mining environments, the orientation of sensors may not be known. In field experi-

ments, local site effects may be significant, distorting systematically the wave amplitudes and masking the real signature of the source.

In this paper, we show how to determine station amplifications in order to fix and overcome the previously discussed difficulties and subsequently to retrieve accurate moment tensors. The method is based on the joint inversion of amplitudes of a family of seismic events for their moment tensors and amplifications of uncalibrated stations. The method works with data either partly or fully recorded by stations of unknown polarity, amplification, or orientation. The method is also suitable for detecting technical problems at the stations, for quantifying local site effects produced by a shallow subsurface structure, for unifying networks equipped with different instruments (e.g., networks combining permanent and mobile stations, short-period and broadband stations, etc.), and, in general, for adjusting seismic networks to retrieve highly accurate moment tensors.

The presented method is tested using numerical modeling. Synthetic tests on data with various noise levels, station configurations, and focal mechanisms are performed in order to validate the robustness and accuracy of the procedure.

Finally, the method is applied to data recorded during the 2008 earthquake swarm in West Bohemia, Czech Republic (Fischer *et al.*, 2010; Vavryčuk, 2011a, b), in order to calibrate the West Bohemia Network (WEBNET) of 22 local seismic stations operating in this region and to improve the accuracy of the moment tensors.

In the following text, the term station amplification will be used and intended as a general term encompassing not only the instrumental amplifications of the sensor and the gain factor of the acquisition system but also the local site effects and other wave propagation effects neglected in the modeling of Green's functions. In the formulas, lower-case bold letters denote row, or column, vectors, and capital bold letters denote matrices. The bold  $\mathbf{0}$  denotes the matrix of zeros, and matrix  $\mathbf{I}$  is the identity matrix.

### Method

The standard procedure is to perform the moment-tensor inversion separately for individual earthquakes. The basic principle of the proposed approach is to perform a joint inversion for moment tensors involving a set of earthquakes. In this way, the number of equations solved in the inversion is increased, and the problem remains overdetermined even if some station amplifications are unknown. In principle, if a large set of earthquakes is analyzed, it is sufficient to know the amplification of just one station in the inversion; the other stations can be of an unknown amplification. Even in this extreme case, we can invert for full-moment tensors including their absolute values (i.e., the scalar moments). If the amplification is unknown for all stations, we can still invert for the moment tensors, but we recover reliably their relative values only (e.g., we cannot estimate the scalar moments of the events).

In this section, we derive equations for station amplifications for three special cases: a network of one-component stations with unknown amplifications, a network of three-component stations with unknown amplifications, and a network of one-component stations with unknown orientations of sensors and unknown amplifications.

#### Network of One-Component Seismic Stations

The system of equations of the standard moment-tensor inversion of amplitudes for one event reads in matrix notation

$$\mathbf{G}\mathbf{m} = \mathbf{u}, \quad (1)$$

in which  $\mathbf{G}$  is the  $N \times 6$  matrix of Green's function amplitudes,

$$\mathbf{G} = \begin{bmatrix} \mathbf{g}^{(1)} \\ \mathbf{g}^{(2)} \\ \vdots \\ \mathbf{g}^{(N)} \end{bmatrix} = \begin{bmatrix} G_1^{(1)} & G_2^{(1)} & G_3^{(1)} & G_4^{(1)} & G_5^{(1)} & G_6^{(1)} \\ G_1^{(2)} & G_2^{(2)} & G_3^{(2)} & G_4^{(2)} & G_5^{(2)} & G_6^{(2)} \\ \vdots & \vdots & \vdots & \vdots & \vdots & \vdots \\ G_1^{(N)} & G_2^{(N)} & G_3^{(N)} & G_4^{(N)} & G_5^{(N)} & G_6^{(N)} \end{bmatrix}, \quad (2)$$

$\mathbf{m}$  is the moment vector composed of six components of moment tensor  $\mathbf{M}$ ,

$$\mathbf{m} = [M_{11} \quad M_{22} \quad M_{33} \quad M_{23} \quad M_{13} \quad M_{12}]^T, \quad (3)$$

and  $\mathbf{u}$  is the vector of displacement amplitudes observed at  $N$  stations,

$$\mathbf{u} = [u^{(1)} \quad u^{(2)} \quad \dots \quad u^{(N)}]^T. \quad (4)$$

Quantities  $G_j^{(i)}$  in equation (2) denote the spatial derivatives of Green's tensor calculated for the  $i$ th station. For example,  $G_j^{(i)}$  are defined for the vertical sensors in the following way:

$$\begin{aligned} G_1 &= G_{31,1}, & G_2 &= G_{32,2}, & G_3 &= G_{33,3}, \\ G_4 &= G_{32,3} + G_{33,2}, & G_5 &= G_{31,3} + G_{33,1}, \\ G_6 &= G_{31,2} + G_{32,1}, \end{aligned} \quad (5)$$

where the superscript ( $i$ ) identifying the station is omitted.

If we incorporate one uncalibrated station with index  $i = N + 1$  into the inversion, we can put

$$\mathbf{g}^{(N+1)}\mathbf{m} = C^{(N+1)}\mathbf{u}^{(N+1)}, \quad (6)$$

where  $C^{(N+1)}$  is the unknown station amplification, and  $\mathbf{g}^{(N+1)}$  is defined as follows:

$$\mathbf{g}^{(N+1)} = [G_1^{(N+1)} \quad G_2^{(N+1)} \quad G_3^{(N+1)} \quad G_4^{(N+1)} \quad G_5^{(N+1)} \quad G_6^{(N+1)}]. \quad (7)$$

By combining equations (1) and (6), we obtain the following equation for moment vector  $\mathbf{m}$  and amplification  $C^{(N+1)}$ :

$$\begin{bmatrix} \mathbf{G} & \mathbf{0} \\ \mathbf{g}^{(N+1)} & -\mathbf{u}^{(N+1)} \end{bmatrix} \cdot \begin{bmatrix} \mathbf{m} \\ C^{(N+1)} \end{bmatrix} = \begin{bmatrix} \mathbf{u} \\ 0 \end{bmatrix}. \quad (8)$$

Obviously, equation (8) can be generalized to solve jointly for the moment tensors of a set of events and for the amplifications of a set of stations. For example, the system of equations for two events recorded at  $N$  calibrated stations and at two uncalibrated stations reads:

$$\begin{bmatrix} \mathbf{G}_{(1)} & 0 & 0 & 0 \\ 0 & \mathbf{G}_{(2)} & 0 & 0 \\ \mathbf{g}_{(1)}^{(N+1)} & 0 & -\mathbf{u}_{(1)}^{(N+1)} & 0 \\ \mathbf{g}_{(1)}^{(N+2)} & 0 & 0 & -\mathbf{u}_{(1)}^{(N+2)} \\ 0 & \mathbf{g}_{(2)}^{(N+1)} & -\mathbf{u}_{(2)}^{(N+1)} & 0 \\ 0 & \mathbf{g}_{(2)}^{(N+2)} & 0 & -\mathbf{u}_{(2)}^{(N+2)} \end{bmatrix} \cdot \begin{bmatrix} \mathbf{m}_{(1)} \\ \mathbf{m}_{(2)} \\ C^{(N+1)} \\ C^{(N+2)} \end{bmatrix} = \begin{bmatrix} \mathbf{u}_{(1)} \\ \mathbf{u}_{(2)} \\ 0 \\ 0 \\ 0 \\ 0 \end{bmatrix}. \quad (9)$$

Analogously, the system of equations for  $L$  seismic events recorded at  $N$  calibrated stations and at  $K - N$  uncalibrated stations takes the following form:

$$\begin{bmatrix} \mathbf{G}_{(1)}^{(1:N)} & \mathbf{0} & \dots & \mathbf{0} & \mathbf{0} \\ \mathbf{0} & \mathbf{G}_{(2)}^{(1:N)} & \dots & \mathbf{0} & \mathbf{0} \\ \dots & \dots & \dots & \dots & \dots \\ \mathbf{0} & \mathbf{0} & \dots & \mathbf{G}_{(L)}^{(1:N)} & \mathbf{0} \\ \mathbf{G}_{(1)}^{(N+1:K)} & \mathbf{0} & \dots & \mathbf{0} & -\mathbf{U}_{(1)}^{(N+1:K)} \\ \mathbf{0} & \mathbf{G}_{(2)}^{(N+1:K)} & \dots & \mathbf{0} & -\mathbf{U}_{(2)}^{(N+1:K)} \\ \dots & \dots & \dots & \dots & \dots \\ \mathbf{0} & \mathbf{0} & \dots & \mathbf{G}_{(L)}^{(N+1:K)} & -\mathbf{U}_{(L)}^{(N+1:K)} \end{bmatrix} \cdot \begin{bmatrix} \mathbf{m}_{(1)} \\ \mathbf{m}_{(2)} \\ \dots \\ \mathbf{m}_{(L)} \\ \mathbf{c}^{(N+1:K)} \end{bmatrix} = \begin{bmatrix} \mathbf{u}_{(1)}^{(1:N)} \\ \mathbf{u}_{(2)}^{(1:N)} \\ \dots \\ \mathbf{u}_{(L)}^{(1:N)} \\ \mathbf{0} \\ \mathbf{0} \\ \dots \\ \mathbf{0} \end{bmatrix}, \quad (10)$$

in which

$$\mathbf{G}_{(i)}^{(m:n)} = \begin{bmatrix} \mathbf{g}_{(i)}^{(m)} \\ \mathbf{g}_{(i)}^{(m+1)} \\ \dots \\ \mathbf{g}_{(i)}^{(n)} \end{bmatrix} = \begin{bmatrix} G_{(i)1}^{(m)} & G_{(i)2}^{(m)} & G_{(i)3}^{(m)} & G_{(i)4}^{(m)} & G_{(i)5}^{(m)} & G_{(i)6}^{(m)} \\ G_{(i)1}^{(m+1)} & G_{(i)2}^{(m+1)} & G_{(i)3}^{(m+1)} & G_{(i)4}^{(m+1)} & G_{(i)5}^{(m+1)} & G_{(i)6}^{(m+1)} \\ \dots & \dots & \dots & \dots & \dots & \dots \\ G_{(i)1}^{(n)} & G_{(i)2}^{(n)} & G_{(i)3}^{(n)} & G_{(i)4}^{(n)} & G_{(i)5}^{(n)} & G_{(i)6}^{(n)} \end{bmatrix}, \quad (11)$$

$$\mathbf{U}_{(i)}^{(m:n)} = \begin{bmatrix} u_{(i)}^{(m)} & 0 & \dots & 0 \\ 0 & u_{(i)}^{(m+1)} & \dots & 0 \\ \dots & \dots & \dots & \dots \\ 0 & 0 & \dots & u_{(i)}^{(n)} \end{bmatrix} \text{ and } \mathbf{c}^{(m:n)} = \begin{bmatrix} C^{(m)} \\ C^{(m+1)} \\ \dots \\ C^{(n)} \end{bmatrix}. \quad (12)$$

Subscript ( $i$ ) denotes the quantity corresponding to the  $i$ th event; superscript ( $m$ ) denotes the quantity corresponding to the  $m$ th station;  $L$  is the total number of events used in the inversion;  $K$  is the total number of stations; and  $N$  is the number of calibrated stations,  $N < K$ . Hence, equation (10) represents equations for the moment tensors of  $L$  events (i.e.,  $6L$  moment tensor components) and for  $M$  station amplifications,  $M = K - N$ . The input is formed by  $L \times K$  amplitudes measured for  $L$  events at  $K$  stations. The amplitudes of each event must be normalized in order to maintain identical weights for all events, irrespective of their magnitudes.

For purposes of illustration, if 10 events recorded at 10 one-component calibrated stations are inverted for their

moment tensors, equation (10) represents a system of 100 equations for 60 unknowns that is a well overdetermined problem. Moreover, such a system of equations is decoupled and can be solved separately for each event. However, if 10 events recorded at one calibrated station and at nine uncalibrated stations are inverted for both their moment tensors and station amplifications, equation (10) represents a system of 100 equations for 69 unknowns. In this case, the system of equations becomes coupled and cannot be disintegrated, but it is still an overdetermined problem.

Note that, in principle, all stations of a seismic network can be of an unknown amplification in equation (10), and we can still invert for moment tensors and for the station amplifications. In this case, the inversion will yield the relative values of the moment tensors and relative station amplifications only. The scalar moments of the events and the absolute amplifications of the stations cannot be estimated.

### Network of Three-Component Seismic Stations

If the seismic network consists of three-component stations, we can either treat each component as an independent one-component station and directly apply equation (10) for the joint inversion for moment tensors and station amplifications, or we can assume just one amplification for each three-component station by modifying equations (11) and (12) in the following way:

$$\mathbf{G}_{(i)}^{(m:n)} = \begin{bmatrix} G_{(i)11}^{(m)} & G_{(i)12}^{(m)} & G_{(i)13}^{(m)} & G_{(i)14}^{(m)} & G_{(i)15}^{(m)} & G_{(i)16}^{(m)} \\ G_{(i)21}^{(m)} & G_{(i)22}^{(m)} & G_{(i)23}^{(m)} & G_{(i)24}^{(m)} & G_{(i)25}^{(m)} & G_{(i)26}^{(m)} \\ G_{(i)31}^{(m)} & G_{(i)32}^{(m)} & G_{(i)33}^{(m)} & G_{(i)34}^{(m)} & G_{(i)35}^{(m)} & G_{(i)36}^{(m)} \\ G_{(i)11}^{(m+1)} & G_{(i)12}^{(m+1)} & G_{(i)13}^{(m+1)} & G_{(i)14}^{(m+1)} & G_{(i)15}^{(m+1)} & G_{(i)16}^{(m+1)} \\ G_{(i)21}^{(m+1)} & G_{(i)22}^{(m+1)} & G_{(i)23}^{(m+1)} & G_{(i)24}^{(m+1)} & G_{(i)25}^{(m+1)} & G_{(i)26}^{(m+1)} \\ G_{(i)31}^{(m+1)} & G_{(i)32}^{(m+1)} & G_{(i)33}^{(m+1)} & G_{(i)34}^{(m+1)} & G_{(i)35}^{(m+1)} & G_{(i)36}^{(m+1)} \\ \dots & \dots & \dots & \dots & \dots & \dots \\ G_{(i)11}^{(n)} & G_{(i)12}^{(n)} & G_{(i)13}^{(n)} & G_{(i)14}^{(n)} & G_{(i)15}^{(n)} & G_{(i)16}^{(n)} \\ G_{(i)21}^{(n)} & G_{(i)22}^{(n)} & G_{(i)23}^{(n)} & G_{(i)24}^{(n)} & G_{(i)25}^{(n)} & G_{(i)26}^{(n)} \\ G_{(i)31}^{(n)} & G_{(i)32}^{(n)} & G_{(i)33}^{(n)} & G_{(i)34}^{(n)} & G_{(i)35}^{(n)} & G_{(i)36}^{(n)} \end{bmatrix}, \quad (13)$$

$$\mathbf{U}_{(i)}^{(m:n)} = \begin{bmatrix} \mathbf{u}_{(i)}^{(m)} & \mathbf{0} & \dots & \mathbf{0} \\ \mathbf{0} & \mathbf{u}_{(i)}^{(m+1)} & \dots & \mathbf{0} \\ \dots & \dots & \dots & \dots \\ \mathbf{0} & \mathbf{0} & \dots & \mathbf{u}_{(i)}^{(n)} \end{bmatrix} \text{ and } \mathbf{u}_{(j)}^{(m)} = \begin{bmatrix} u_{(j)1}^{(m)} \\ u_{(j)2}^{(m)} \\ u_{(j)3}^{(m)} \end{bmatrix}, \quad (14)$$

in which

$$\begin{aligned}
 G_{11} &= G_{11,1}, & G_{12} &= G_{12,2}, & G_{13} &= G_{13,3}, \\
 G_{14} &= G_{12,3} + G_{13,2}, & G_{15} &= G_{11,3} + G_{13,1}, \\
 G_{16} &= G_{11,2} + G_{12,1},
 \end{aligned}
 \tag{15}$$

and analogously for the other components  $G_{kl}$ , where superscript ( $m$ ) identifying the station and subscript ( $i$ ) identifying the event have been omitted.

### Network of Seismic Stations with Unknown Orientations of Sensors

Let us assume a seismic network of one-component stations, some of them being uncalibrated and oriented in an unknown direction. In this case, the inversion can be used to calculate the moment tensors, as well as the station amplifications and orientations. For simplicity, let us assume a seismic event recorded at  $N$  one-component calibrated stations and at one uncalibrated station with an unknown orientation. The equation for the uncalibrated/misoriented station reads

$$\mathbf{G}^{(N+1)} \mathbf{m} = \mathbf{c}^{(N+1)} u^{(N+1)},
 \tag{16}$$

in which  $\mathbf{m}$  is the moment vector,  $u^{(N+1)}$  is the displacement amplitude at the uncalibrated station,  $\mathbf{G}^{(N+1)}$  is the matrix of Green's function amplitudes for the uncalibrated station,

$$\mathbf{G}^{(N+1)} = \begin{bmatrix} G_{11}^{(N+1)} & G_{12}^{(N+1)} & G_{13}^{(N+1)} & G_{14}^{(N+1)} & G_{15}^{(N+1)} & G_{16}^{(N+1)} \\ G_{21}^{(N+1)} & G_{22}^{(N+1)} & G_{23}^{(N+1)} & G_{24}^{(N+1)} & G_{25}^{(N+1)} & G_{26}^{(N+1)} \\ G_{31}^{(N+1)} & G_{32}^{(N+1)} & G_{33}^{(N+1)} & G_{34}^{(N+1)} & G_{35}^{(N+1)} & G_{36}^{(N+1)} \end{bmatrix},
 \tag{17}$$

and  $\mathbf{c}^{(N+1)}$  is the amplification vector of the uncalibrated station, which defines the amplifications along the three coordinate axes,

$$\mathbf{c}^{(N+1)} = \begin{bmatrix} c_1^{(N+1)} \\ c_2^{(N+1)} \\ c_3^{(N+1)} \end{bmatrix}.
 \tag{18}$$

Amplification vector  $\mathbf{c}^{(N+1)}$  can be decomposed into scalar amplification  $C^{(N+1)}$  and unit direction vector  $\mathbf{n}^{(N+1)}$  defining the orientation of the sensor as

$$C = \sqrt{c_k c_k}, \quad \mathbf{n} = \frac{\mathbf{c}}{C},
 \tag{19}$$

in which the superscript ( $N + 1$ ) is omitted. Combining equations (1) and (16) we obtain the following equation for moment vector  $\mathbf{m}$  and for amplification vector  $\mathbf{c}^{(N+1)}$ :

$$\begin{bmatrix} \mathbf{G} & \mathbf{0} \\ \mathbf{G}^{(N+1)} & -u^{(N+1)} \mathbf{I} \end{bmatrix} \cdot \begin{bmatrix} \mathbf{m} \\ \mathbf{c}^{(N+1)} \end{bmatrix} = \begin{bmatrix} \mathbf{u} \\ \mathbf{0} \end{bmatrix},
 \tag{20}$$

in which  $\mathbf{I}$  is the  $3 \times 3$  identity matrix. Analogously, as in the previous calibration approaches, equation (20) can be generalized for inverting  $L$  seismic events recorded at  $N$  calibrated stations and  $M$  uncalibrated/misoriented stations.

For illustration, if 10 events recorded at nine one-component calibrated stations and at one uncalibrated/misoriented station are inverted for moment tensors, we solve a system of 100 equations for 63 unknowns (60 moment tensor components plus three station amplifications), which is a well overdetermined problem. If 10 events recorded at one calibrated station and at nine uncalibrated/misoriented stations are inverted for moment tensors and station amplifications and orientations, we solve a system of 100 equations for 87 unknowns (60 moment tensor components plus 27 station amplifications), which is still an overdetermined problem.

### Network Calibration Strategies

In order to obtain reliable and accurate seismic network station amplifications, the derived systems of equations discussed previously must be well overdetermined and their inversion must be stable. This requires satisfaction of the following conditions: (1) The seismic network must be sufficiently dense to ensure good focal sphere coverage. (2) The technical parameters of the stations and their in-situ installation must not change in the analyzed dataset. (3) The inverted amplitudes must have a good signal-to-noise ratio. (4) The velocity model and the event locations must be sufficiently accurate. (5) Extensive datasets of seismic events must be inverted. (6) The events should display a variety of focal mechanisms. Conditions (1)–(4) are standard conditions of any reliable moment-tensor inversion; conditions (5)–(6) are additional conditions needed for reliable network calibration.

### Partial Network Calibration

Initially, we consider a case in which just one or several stations of the network are problematic, having unknown polarity, orientation or calibration. If the core of the network is well calibrated and well installed, we can fix the core stations in the inversion and apply the derived systems of equations previously discussed to calibrating a part of the network only. Obviously, the retrieved amplifications of the calibrating stations will comprise the reverse polarity, the instrumental amplification of the sensors, the gain factor of the acquisition system, and additionally the local site effects at the individual stations. Therefore, it is recommended also that calibrations be performed for stations recording wavefields presumably affected by the site effects neglected in calculations of Green's functions. The accuracy of the station amplifications can be estimated using the standard tools: (1) a jackknife test, when we invert for the station amplifications using randomly

selected subsets of the seismic events, or (2) a repeated inversion of noisy data when amplitudes are contaminated by random noise, and Green's functions are calculated using slightly different velocity models and biased event locations.

### Complete Network Calibration

An alternative to calibrating selected stations only is a complete network calibration, which is particularly desirable when performed as the final step of the process when the amplifications of the most problematic stations have been retrieved by partial network calibration. Complete network calibration can adjust station amplifications by including the local site effects at all stations produced by shallow subsurface structures or by the rock-sensor coupling and all other wave propagation effects neglected in calculating Green's functions. The calibration reveals systematic discrepancies in amplitudes at the stations and optimizes the moment-tensor inversion. As a result, the root-mean-square (rms) differences between observed and calculated amplitudes are reduced in average, and the accuracy of the moment tensors is improved.

The simplest way of calibrating the complete network consisting of  $N$  stations is to perform the calibration in iterations in the following way (Fig. 1):

- (1) We fix the station amplifications at  $N - 1$  stations at the original, actually used values or values obtained using the partial network calibration and calibrate just one remnant station.
- (2) We successively repeat step (1) with different station configurations  $N$  times, finally obtaining corrected station amplifications at all  $N$  stations.
- (3) The set of corrected station amplifications is normalized in order to maintain the overall amplification of the entire network.
- (4) Steps (1) through (3) constitute a single iteration. The iterations are successively repeated.
- (5) For each iteration, we calculate the difference between the station amplifications obtained in two successive iterations.
- (6) The calibration process is stopped when the new iteration does not change the station amplifications calculated in the previous iteration by a value higher than a prescribed limit or if the number of iterations exceeds a prescribed maximum value.

The convergence of the iterations can be improved if we use a better and more accurate initial guess of the station amplifications in the iteration process. For example, Figure 2 shows a procedure in which we fix the amplification at one station and calculate the amplifications across the remainder of the network. This is repeated for each individual station of the network; hence, we obtain  $N$  sets of  $N$  station amplifications. The  $N$  amplifications for each station are then averaged and fixed as the initial guess in the iterative process. This

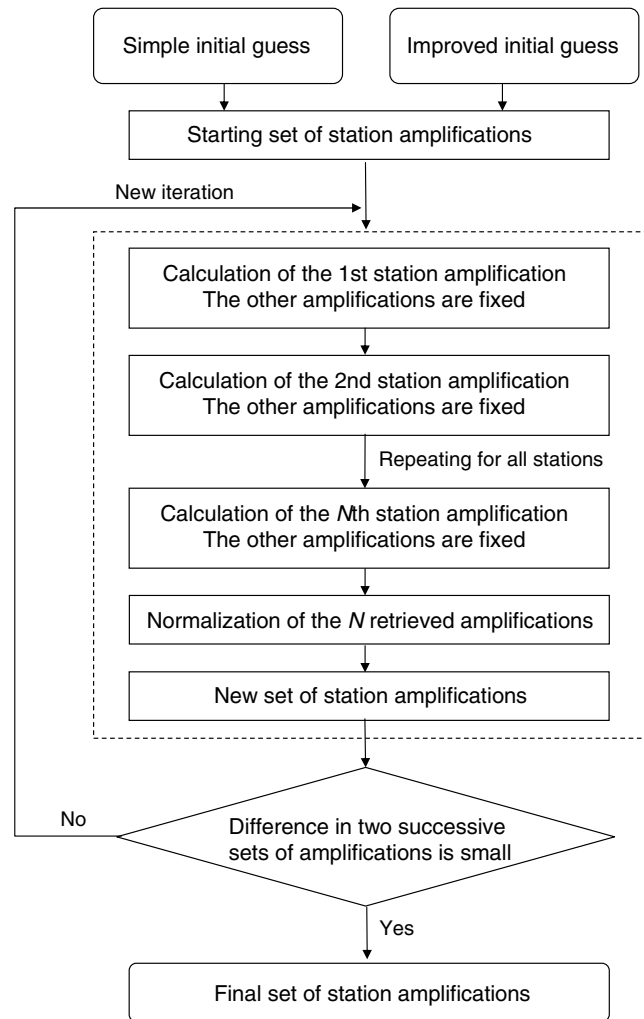


**Figure 1.** Flowchart of the iterative complete network calibration. The dashed-line frame identifies one iteration.

approach will be called the improved initial guess in order to distinguish it from the simple initial guess when the starting values of the station amplifications are assumed to be the original station amplifications.

The accuracy of the final station amplifications can be estimated similarly as in the case of the partial network calibration, i.e., by the jackknife test in which we invert for the station amplifications using randomly selected subsets of seismic events or by repeated inversions of noisy data with biased velocity models and biased event locations.

### Numerical Tests

In order to test the robustness of the proposed inversion scheme, we performed a series of synthetic tests. By generating datasets of events with synthetic focal mechanisms, we calculated synthetic vertical  $P$ -wave amplitudes using the ray method, contaminated them by noise, and multiplied them by synthetic station amplifications. We then applied the

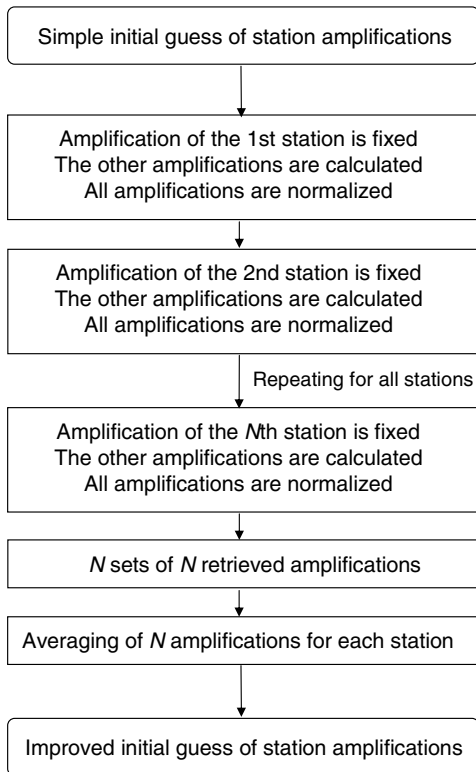


**Figure 2.** Flowchart of the improved initial guess of station amplifications used in the iterative complete network calibration.

procedure of calibrating the network and retrieving the moment tensors. The event locations, velocity model, and the network configuration were used to mimic seismic observations in the West Bohemia region, Czech Republic (see [Application to the West Bohemia Seismic Network \[WEBNET\]](#)).

### Synthetic Datasets

We utilized three different datasets consisting of 10, 50, and 200 events with two station configurations defined as the sparse and dense configuration. Both these configurations recall the real distribution of stations deployed in the West Bohemia region (Fig. 3). The sparse and dense configurations comprise 10 and 22 stations, respectively (Fig. 4). The synthetic vertical  $P$ -wave amplitudes were contaminated with uniformly distributed random noise of three levels: up to 10%, 25%, and 50% of the noise-free amplitude. The synthetic focal mechanisms were pure shear with the orientation close to the characteristic focal mechanism in the West Bohemia region, also referred to as the principal focal mechanism shown in Figure 4. The mechanism is defined by a strike of  $169^\circ$ , a dip of  $68^\circ$ , and a rake of  $-44^\circ$ , and its orientation is optimum for shear faulting under tectonic stress in the region (see [Vavryčuk, 2011a](#)). The deviation of the mechanisms from the principal focal mechanism is random, reaching values of up to  $20^\circ$  in strike, dip, and rake angles (Fig. 5). The depth of the hypocenters is between 7.5

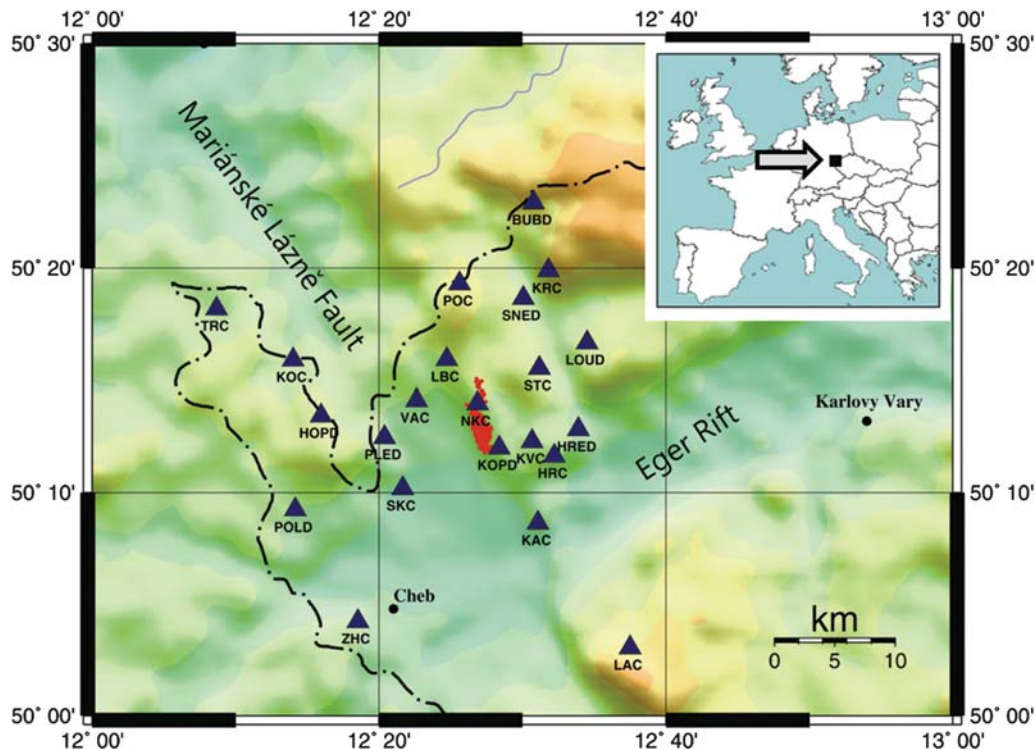


**Figure 3.** Topographic map of the West Bohemia/Vogtland region. The epicenters of the 2008 swarm micro-earthquakes are marked by red dots, and the WEBNET stations are marked by blue triangles. The dashed-dotted line shows the border between the Czech Republic and Germany.

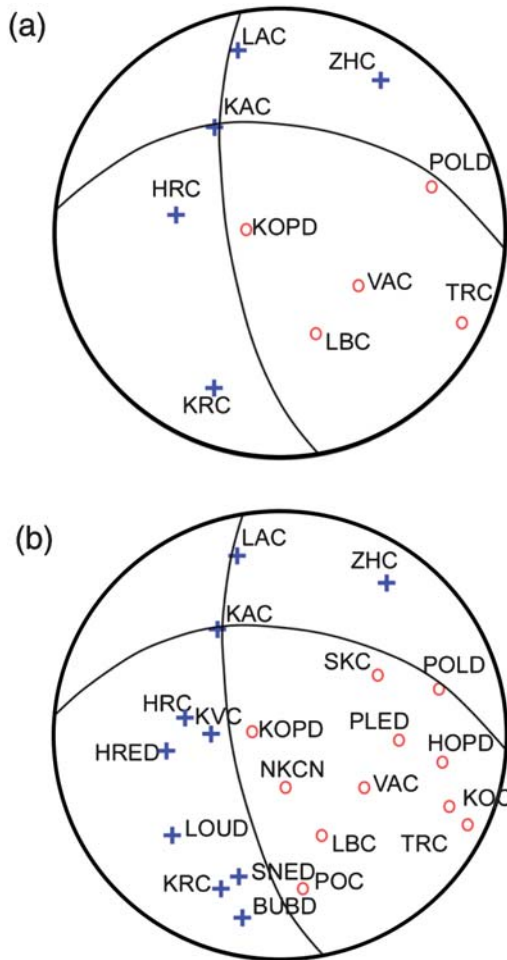


**Figure 4.** (a) Sparse and (b) dense station configurations. Red circles and blue plus-signs indicate positions of stations on the focal sphere and their negative and positive *P*-wave polarities, respectively. The nodal lines and *P*-wave polarities at the stations correspond to the principal focal mechanism, which characterizes the majority of micro-earthquakes observed in West Bohemia (Vavryčuk, 2011a).

and 11.0 km, a 1D layered velocity model is used, and the epicentral distances of the stations are up to 30 km.

**Partial Network Calibration**

Initially, we test the procedure for the partial network calibration and fix the core of the network with differently selected configurations. For the sparse configuration, we alternatively fix 1 and 5 stations considered to be well calibrated and well installed, while the amplifications of the remaining stations are retrieved by the inversion. For the dense configuration, the core of the network, with 1, 5, and 10 stations, is alternatively fixed.

The inversion for the station amplifications is repeated 100 times for different randomly generated noise and, subsequently, the relative errors of the retrieved station amplifications are calculated from the standard deviations. The results are summarized in Table 1 and shown in Figures 6

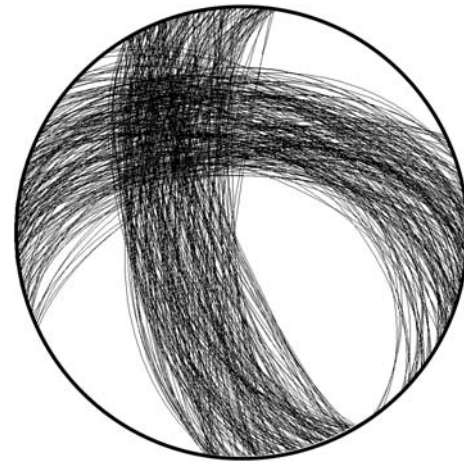


**Figure 5.** Focal mechanisms of 200 synthetic pure shear events randomly distributed around the principal focal mechanism. The deviation of strike, dip, and rake is up to 20° from the principal focal mechanism shown in Figure 4.

**Table 1**  
Accuracy of Station Amplifications—Numerical Modeling

Events	Fixed Stations	Noise Level (%)	$E_{\text{sparse}}$ (%)	$E_{\text{dense}}$ (%)
10	1	10	7.2	4.1
		25	16.4	8.5
		50	26.0	16.9
50	1	10	3.1	1.7
		25	7.1	4.5
		50	11.3	6.3
200	1	10	1.7	0.9
		25	3.1	2.4
		50	4.7	4.0
10	5	10	3.4	2.9
		25	7.2	7.1
		50	14.8	12.5
50	5	10	1.2	1.3
		25	3.1	2.9
		50	5.3	4.9
200	5	10	0.8	0.7
		25	2.2	1.8
		50	3.9	2.8
10	10	10	–	2.2
		25	–	5.6
		50	–	10.5
50	10	10	–	0.9
		25	–	2.3
		50	–	4.2
200	10	10	–	0.5
		25	–	1.6
		50	–	2.9

Events: the number of events used in the inversion; fixed stations: the number of core stations with fixed amplifications; noise level: the maximum relative level of noise superimposed to *P*-wave amplitudes used in the inversion,  $E_{\text{sparse}}$  and  $E_{\text{dense}}$ , the relative errors of the retrieved station amplifications averaged over all inverted stations and over all generations of random noise for sparse and dense station configurations, respectively.

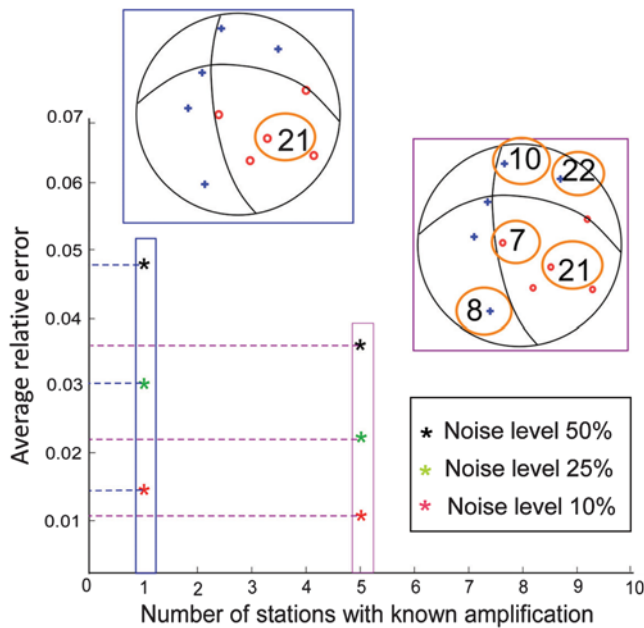


**Figure 6.** Relative error (in %) of the retrieved station amplifications for the sparse station configuration. The station amplifications are calculated using noisy amplitudes of 200 events. The errors are averaged over 100 generations of random noise and over 9 (blue box and column) and 5 (pink box and column) inverted stations, respectively. The figure shows two different configurations of the core network with 1 (blue box and column) and 5 (pink box and column) core stations with a fixed amplification. The black, green, and red stars correspond to the noise levels of 50%, 25%, and 10%, respectively. The core stations with the fixed amplifications are circled on the focal spheres. The numbers identifying the stations are given in Table 4.

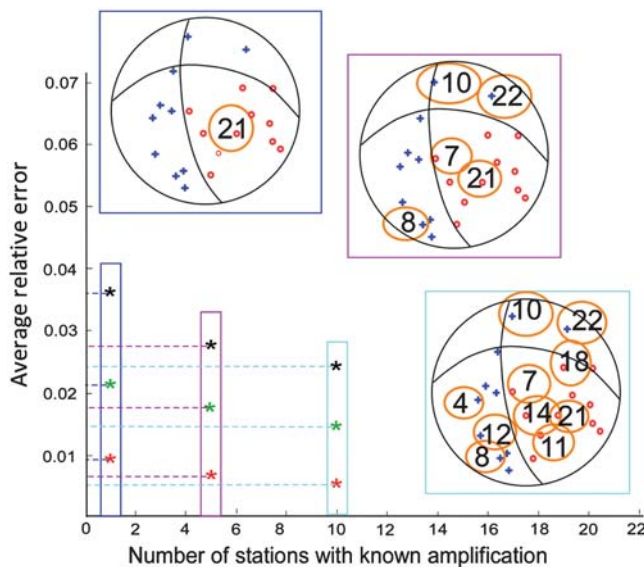


**Figure 7.** Same as Figure 6 but for the dense station configuration and for three configurations of the core network with 1, 5, and 10 core stations with a fixed amplification.

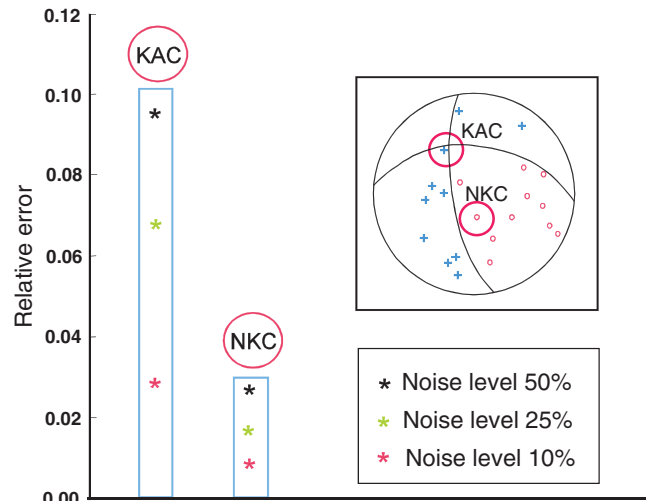


**Figure 8.** Relative error (in %) of the station amplifications calculated for the KAC and NKC stations for the dense station configuration. The station amplifications are calculated using noisy amplitudes of 200 events. The errors are averaged over 100 generations of random noise. The calibration is performed for a network with 1 core station (VAC) with a fixed amplification. The errors are high for the unfavorably positioned KAC station and low for the favorably positioned NKC station.

and 7. The table and the figures confirm that the inversion code works well and yields robust results. As expected, the inversion code performs better with a high number of stations with known amplifications, a low level of noise, and a high number of jointly analyzed events. In these cases, the inversion yields smaller amplification errors. Figures 6 and 7 show the results for 200 events, but basically, the same trends are obtained for datasets with other numbers of events.

We also performed sensitivity tests with regard to the position of the stations on the focal sphere and to a variety of focal mechanisms of analyzed events. The tests show that the station amplifications are better resolved for datasets with a higher variety of focal mechanisms. If the focal mechanisms are very similar or identical, then equation (10) consists of linearly dependent equations, and the inversion either fails or yields low accuracy results. Moreover, the accuracy of the station amplifications depends on the station position on the focal sphere. Stations located in the proximity of the nodal lines display higher errors compared with the other stations (Fig. 8). If the condition of a variety of focal mechanisms is satisfied, the inversion yields accurate results independent of the station locations. Another possibility of improving the accuracy of amplifications and decreasing their sensitivity to the station’s positions on the focal sphere is to include S-wave amplitudes in the inversion.

### Complete Network Calibration

Finally, we perform synthetic tests of the complete network calibration in order to assess its robustness, stability,

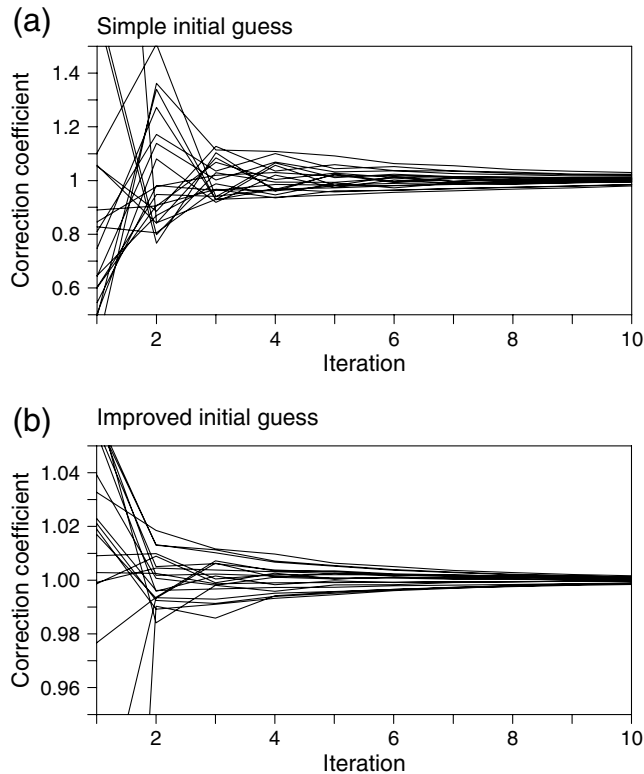


**Figure 9.** Convergence of the iterative complete network calibration using 200 synthetic events and a noise level of 25%: (a) the simple initial guess approach, and (b) the improved initial guess approach. The correction coefficient represents the multiplication factor needed for obtaining the amplification in the next iteration from its value calculated in the previous iteration. High and low values of the correction coefficient for several first iterations are clipped for some stations. Value 1 of the correction coefficient means that the two successive iterations yield the same amplification value with no further improvement. Note that the scale in (b) is 10 times larger than in (a) to see the convergence in detail.

and accuracy by using the dense station configuration (Fig. 4b). The true synthetic station amplifications vary between 0.5 and 2.0 with the mean value being 1. We calculate the synthetic vertical  $P$ -wave amplitudes for all 200 events recorded at all stations. The  $P$ -wave amplitudes are contaminated by a uniformly distributed random noise with a level of up to 25%, which are used as input data for the complete network calibration. We apply an iterative calibration with two different sets of station amplification starting values. First, we assume a simple initial guess when the starting values of all station amplifications equal 1, and second, we estimate the starting values using the improved initial guess as described in [Network Calibration Strategies](#) and in Figure 2. We calculate 25 iterations to obtain accurate station amplifications.

Figure 9 shows the convergence of the iteration process for the two initial guesses. As expected, the iteration process with the improved initial guess converges much faster. In fact, the station amplifications reach their final values after

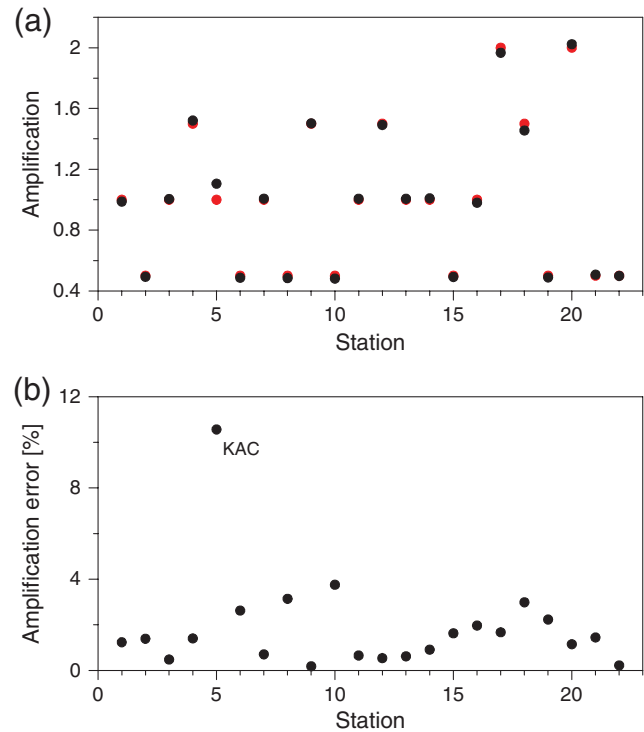


**Figure 10.** (a) True synthetic (red dots) and retrieved (black dots) station amplifications. (b) Relative errors of amplifications calculated as absolute values of the difference between the true and retrieved amplifications in percentages. The network calibrations with the simple and improved initial guesses yield the same retrieved values (black dots) of the station amplifications.

10 iterations, and additional iterations show no practical improvement. As seen from Figure 10a, both iteration procedures converge at the same values (black dots). However, the retrieved amplifications are slightly biased from the true synthetic amplifications (red dots), which is caused by noise in the data. The lowest accuracy is achieved for station KAC (Fig. 10b, station 5), which has an unfavorable position on the focal sphere being very close to the intersection of the nodal lines for the majority of the events (Fig. 4).

Figure 11 shows a comparison of moment tensors calculated from uncalibrated data when station amplifications are assumed to be 1 (uncorrected moment tensors), and from calibrated data when data are corrected by station amplifications retrieved using the complete network calibration (corrected moment tensors). It is worthy to note that the focal mechanisms (left-hand plots) are better clustered for uncalibrated moment tensors. Although the nodal lines appear more clustered, they do not represent the true nodal lines as shown in Figure 5. The most important observation relates to the properties of the non-DC components. The uncorrected moment tensors display significant false negative compensated linear vector dipole (CLVD) and isotropic (ISO) components (Table 2 and Fig. 11, middle plots). The corrected moment tensors display less negative CLVD and

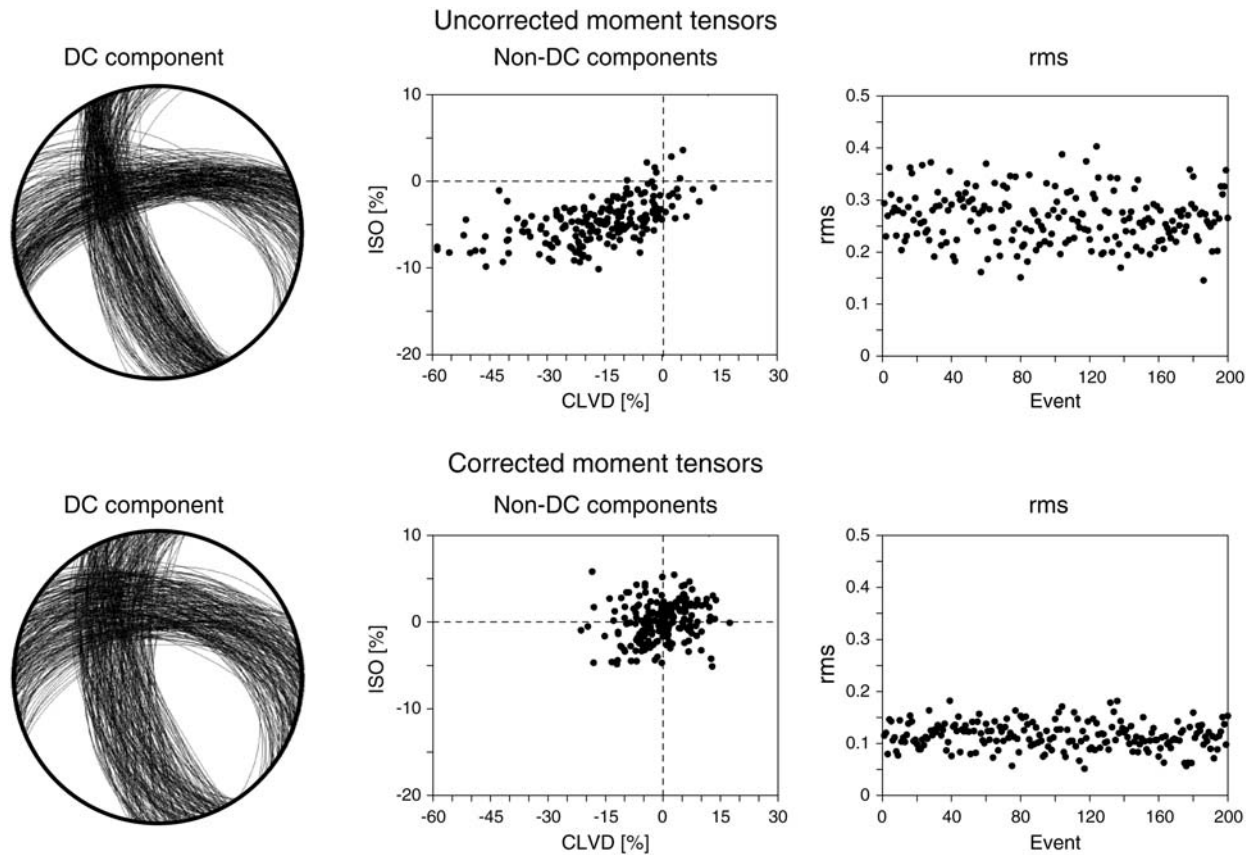


**Figure 11.** The 200 moment tensors retrieved using the uncalibrated (upper plots) and calibrated (lower plots) network. The maximum level of random noise in the  $P$ -wave amplitudes is 25%. The uncorrected moment tensors are calculated from uncalibrated data when station amplifications are assumed to be 1. The corrected moment tensors are calculated from calibrated data when data are corrected by station amplifications retrieved using the complete network calibration (Fig. 10a). The corrected moment tensors display low root-mean-square (rms) values and the non-double-couple (non-DC) components centered in the origin of the isotropic (ISO) and compensated linear vector dipole (CLVD) coordinates (dashed lines in the middle plots). The rms, CLVD and ISO of corrected moment tensors are zero for noise-free data (see Table 2).

ISO components and form a cluster centered on coordinate origin. The size of the cluster depends on the noise level in inverted data (the noise level is 25% in Fig. 11). If the noise level is decreased, the cluster will shrink. Obviously,

the CLVD and ISO of corrected moment tensors become zero for noise-free data. Moreover, we calculate the rms values defined as the normalized differences between the synthetic and observed amplitudes in the moment-tensor inversion:

Table 2  
Moment Tensor Inversion—Numerical Modeling

Dataset	DC (%)	CLVD (%)	ISO (%)	CLVD  (%)	ISO  (%)	rms
Uncorrected moment tensors						
Noise-free data	77.6	-17.2	-4.7	17.7	4.7	0.248
Noisy data	77.5	-17.1	-4.6	17.8	4.8	0.266
Corrected moment tensors						
Noise-free data	100.0	0.0	0.0	0.0	0.0	0.000
Noisy data	92.5	-0.7	0.1	5.6	1.8	0.115

DC, CLVD, and ISO: average double-couple, compensated linear vector dipole, and isotropic percentages, respectively; |CLVD| and |ISO|: average absolute values of the CLVD and ISO percentages; rms: the root-mean-square misfit between the inverted and obtained amplitudes (see equation 21) averaged over all events. The percentages of the DC, CLVD, and ISO are calculated using the formulas of Vavryčuk (2001). The maximum level of random noise in the noisy data is 25%.

$$\text{rms} = \frac{\sqrt{\sum (A_i^{\text{synth}} - A_i^{\text{obs}})^2}}{\sqrt{\sum (A_i^{\text{synth}})^2}}, \quad (21)$$

in which subscript ( $i$ ) defines the station, and the summation is over all stations that recorded the analyzed event. As expected, the rms values are higher for the uncalibrated network in which the average values are  $\sim 0.25$  and  $0.27$  for noise-free and noisy data, respectively (Table 2 and Fig. 11, right-hand plots). The rms values significantly decrease if calculated for moment tensors after calibrating the network: the average values are  $0.12$  for noisy data and zero for noise-free data.

### Application to the West Bohemia Seismic Network (WEBNET)

Because of the high number of stations and excellent station coverage on the focal sphere, the West Bohemia region is suitable for testing the proposed inversion for station amplifications. Since we do not expect serious problems with polarities, amplifications, or orientations of the WEBNET stations, the inversion is used only to check the quality of the network and to identify stations with potential problems mostly caused by site effects related to local geology. Finally, we aim to improve the accuracy of the moment tensors by network calibration.

#### The West Bohemia Swarm Area and the WEBNET Network

The West Bohemia region is characterized by intense seismic activity with frequent occurrence of earthquake swarms (Fischer and Horálek, 2003). One of the most recent and prominent swarms was recorded in October 2008, which lasted for four weeks and included 25,000 micro-earthquakes with magnitudes higher than  $-0.5$  and with the largest event showing a magnitude of  $3.7$ . The epicenters formed a cluster prolonged in the north–south direction of  $4\text{--}5$  km in length (Fig. 3). The hypocenters were located at depths of  $7.5\text{--}11$  km (Fischer *et al.*, 2010). The seismic activity in West Bohemia is thought to be connected to young Quaternary volcanism and is generally linked with mineral water springs with high  $\text{CO}_2$  content (Babuška *et al.*, 2007). The seismicity is monitored by 22 short-period seismic stations of the West Bohemia Network (WEBNET), see Figure 3. The sampling frequency is  $250$  Hz, and the frequency response is flat between at least  $1.0$  and  $60$  Hz with some variations depending on the seismometer used (SM-3, Guralp CMG-40T, Lennartz Le3D). The majority of events observed in 2008 were characterized by a left-lateral strike slip with a strike of  $169^\circ$ . The other representative focal mechanism is a right-lateral strike slip with a strike of  $304^\circ$  (Vavryčuk, 2011a). The maximum compressive stress determined from the focal mechanisms has an azimuth of  $\text{N}146^\circ\text{E}$  (Vavryčuk, 2011a), which coin-

cides well with the average direction  $\text{N}144^\circ\text{E}$  in Western Europe (Müller *et al.*, 1992; Heidbach *et al.*, 2008).

#### Data

We selected a dataset of 200 micro-earthquakes recorded at least by 20 stations with a high signal-to-noise ratio (5 or more for most stations) and with highly accurate hypocenter locations with errors of less than  $50$  m in the horizontal coordinates and less than  $100$  m in depth. The velocity records were numerically integrated into the displacement records and filtered by a band-pass filter in the frequency range of  $1\text{--}40$  Hz. The predominant frequency of the signal was between  $10$  and  $20$  Hz. The maximum  $P$ -wave amplitudes were measured by an analyst. The vertical components of the  $P$ -wave amplitudes were inverted for full-moment tensors using the standard linear inversion (Vavryčuk, 2011a). Green's functions were calculated for a smooth, vertically inhomogeneous model using the ray method (Červený, 2001) and incorporated the effects of the Earth's surface by considering free-surface conversion coefficients. The full-moment tensors were calculated using the generalized linear inversion of equation (1) and decomposed into DC and non-DC components (Vavryčuk, 2001, 2002). The reliability of the moment tensors was assessed by calculating the rms values using equation (21). The errors of the moment tensors produced by inaccurate locations or by an inaccurate velocity model were estimated to be less than  $4^\circ$  in the orientation of the focal mechanism and  $5\%$  in the non-DC components.

The focal mechanisms of the selected events are basically of two types (Fig. 12b) being close to the two conjugate principal focal mechanisms characteristic for this region and defined by the following angles (see Vavryčuk, 2011a):  $\phi_1 = 169^\circ$ ,  $\delta_1 = 68^\circ$ ,  $\lambda_1 = -44^\circ$ , and  $\phi_2 = 304^\circ$ ,  $\delta_2 = 66^\circ$ ,  $\lambda_2 = -137^\circ$ . The first principal focal mechanism is the oblique left-lateral strike slip (Fig. 12a, red nodal lines). This mechanism is typical for this region, very commonly observed, and the corresponding fault plays an essential role in the seismicity in West Bohemia. The other principal focal mechanism is oblique right-lateral strike slip (Fig. 12a, blue nodal lines). This mechanism is less frequent, but the corresponding fault is well manifested on the Earth's surface. The full-moment tensors of both types of principal focal mechanisms display non-DC components, which are prevalently negative (see Vavryčuk, 2011c). The average values of the ISO and CLVD components are  $-2.3\%$  and  $-16.3\%$ , respectively (see Table 3). The average value of the rms calculated in the moment-tensor inversion of the selected events is  $0.19$  (see Table 3).

#### The WEBNET Network Calibration

The dataset of the 200 selected micro-earthquakes was used for a complete network calibration in order to evaluate the vertical amplifications at each of the 22 stations of the WEBNET network. The iterative procedure was run with

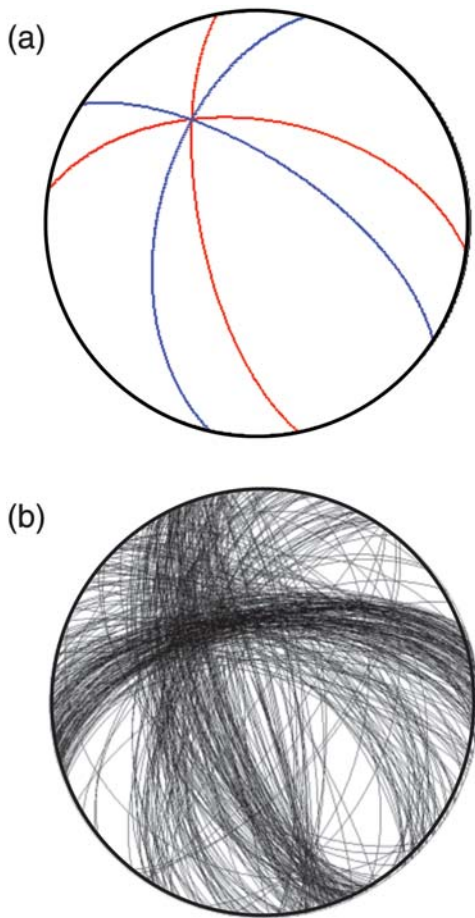


**Figure 12.** (a) Focal mechanisms of two principal earthquakes in West Bohemia, (b) focal mechanisms of 200 micro-earthquakes selected from the 2008 swarm in West Bohemia for calibrating the WEBNET network.

the simple and improved initial guesses of station amplifications. Similarly, as in the numerical modeling, the overall amplification of the entire network was maintained to be constant. The accuracy of the amplification corrections was estimated using the jackknife test when the iterative procedure was run 50 times on subsets of 100 randomly selected events.

Since the variability of the focal mechanisms is higher for observed data (Fig. 12b) than for the synthetic data used

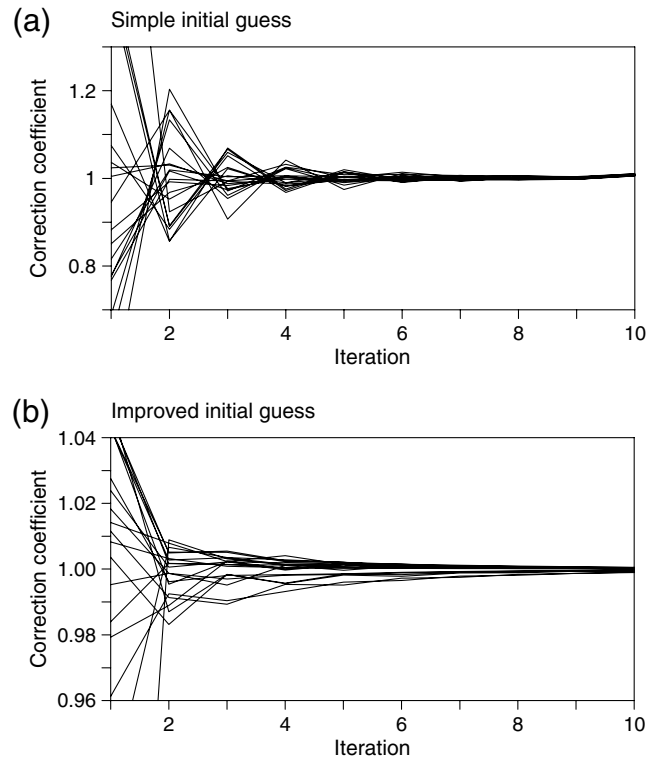


**Figure 13.** Same as Figure 9 but for real observations at the WEBNET network.

in the numerical modeling (Fig. 5), we can expect good convergence of the iterations, as well as a reasonable accuracy of the station amplifications retrieved by the network calibration. The results of the calibration are shown in Figures 13 and 14 and confirm our expectations. As in the numerical modeling, the iterations with the simple and improved initial guess converge at the same values of station amplifications. Also, iterations with the improved initial guess converge faster than those with the simple initial guess (Fig. 13). The achieved accuracy of station amplification is reasonable, being less than 4% for the majority of stations. The only exceptions are stations KAC and HRED with accuracies of 6.0% and 5.6%, respectively (Table 4 and Fig. 14b). The low accuracy of the station amplification for the KAC station is

Table 3  
Moment Tensor Inversion—West Bohemia Data

Dataset	DC (%)	CLVD (%)	ISO (%)	CLVD  (%)	ISO  (%)	rms
Uncorrected moment tensors	76.3	-16.3	-2.3	19.0	4.6	0.191
Corrected moment tensors	83.8	-9.7	-1.5	12.5	3.7	0.112

DC, CLVD, and ISO: average double-couple, compensated linear vector dipole and isotropic percentages, respectively; |CLVD| and |ISO|: average absolute values of the CLVD and ISO percentages; rms: the root-mean-square misfit between the inverted and obtained amplitudes (see equation 21) averaged over all events. The uncorrected moment tensors are calculated using original amplitudes. The corrected moment tensors are calculated using amplitudes of the calibrated network. The percentages of the DC, CLVD, and ISO are calculated using the formulas of Vavryčuk (2001).

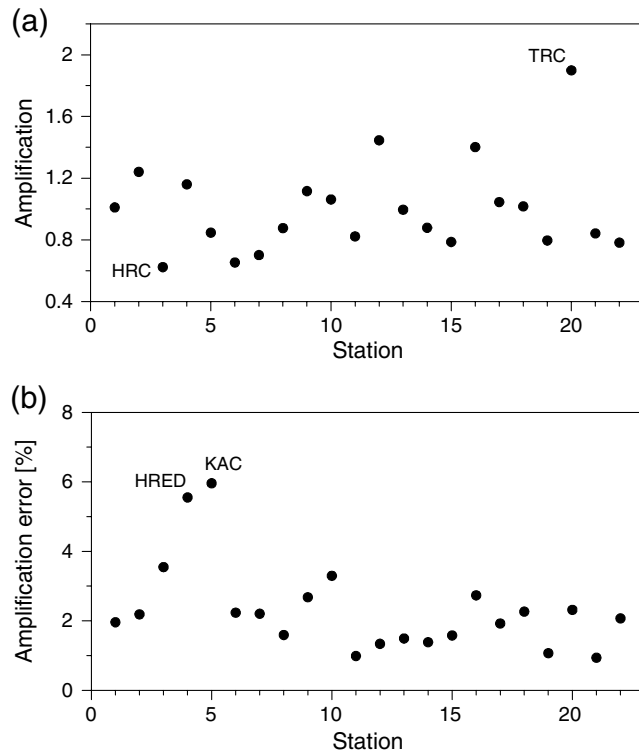


**Figure 14.** Complete calibration of the WEBNET network. (a) Retrieved station amplifications. (b) Relative errors of amplifications calculated as the standard deviations of 50 values obtained by using the jackknife test. The network calibrations with the simple and improved initial guesses yield the same station amplifications (see Table 4 and the text for more details).

likely connected with its unfavorable position on the focal sphere, situated at the intersection of the nodal lines (Fig. 4). The low accuracy for the KAC station also was obtained through numerical modeling (Fig. 10b). The low accuracy for the HRED station is likely due to a generally higher noise level detected at this station in comparison with the other stations.

In regard to the actual values of retrieved amplifications (Table 4 and Fig. 14a), we can summarize the following observations:

- (1) It was confirmed that no station was of a reversed polarity (no amplification correction was negative).
- (2) TRC station (station 20) has an anomalous amplification correction. This indicates either incorrect calibration of the sensor, incorrect value of the gain factor, or an anomalous medium response (i.e., anomalous attenuation of waves).
- (3) The scatter of the amplification corrections of the other stations is surprisingly high: the values range from 0.62 to 1.45 (see Table 4). Such a high scatter of amplification corrections was not expected because (a) the majority of stations should not be affected by any technical problems, and (b) all stations are installed on consolidated rocks, which minimize site effects in wave ampli-

**Table 4**  
WEBNET Network Calibration

Station	Station Name	Amplification Correction	Absolute Error	Relative Error (%)
1	BUBD	1.01	0.02	2.0
2	HOPD	1.24	0.03	2.2
3	HRC	0.62	0.02	3.5
4	HRED	1.16	0.06	5.6
5	KAC	0.85	0.05	6.0
6	KOC	0.65	0.01	2.2
7	KOPD	0.70	0.02	2.2
8	KRC	0.88	0.01	1.6
9	KVC	1.12	0.03	2.7
10	LAC	1.06	0.04	3.3
11	LBC	0.82	0.01	1.0
12	LOUD	1.45	0.02	1.3
13	NKC	1.00	0.01	1.5
14	NKCN	0.88	0.01	1.4
15	PLED	0.79	0.01	1.6
16	POC	1.40	0.04	2.7
17	POLD	1.04	0.02	1.9
18	SKC	1.02	0.02	2.3
19	SNED	0.80	0.01	1.1
20	TRC	1.90	0.04	2.3
21	VAC	0.84	0.01	0.9
22	ZHC	0.78	0.02	2.1

Amplification correction means the multiplication factor needed for correcting the observed amplitudes. The absolute errors are the standard deviations of the 50 amplifications for each station obtained using the jackknife test when the inversion was run 50 times on subsets of 100 events randomly selected from the whole dataset of 200 events.

tudes. Since the retrieved amplifications are stable and accurately determined, the assumption of a minor influence of local site effects must be probably revised.

- (4) A comparison of amplification corrections of stations NKC (1.00) and NKCN (0.88) points also to a non-negligible influence of the type of sensor installed at the station. In fact, station codes NKC and NKCN correspond to the same station recording six channels: three of them being short-period-equipped with the SM-3 seismometers, and the other being broadband-equipped with the Guralp CMG-40T seismometer. Therefore, the difference in amplification corrections must be produced by the different sensors. It is worthy to note that even though the records were uniformly filtered by a band-pass filter to retain only signals in the frequency range of 1.0–40 Hz, the dependence on the sensor was not fully removed. Hence, we can conclude that the variations in amplification can be produced partly by different types of seismometers used in the network.

Note that the amplification corrections were retrieved using waves with a predominant frequency between 10 and 20 Hz. Since the frequency response of the sensors and the site effects can be frequency-dependent, the amplification values might be different if studied in another frequency band.

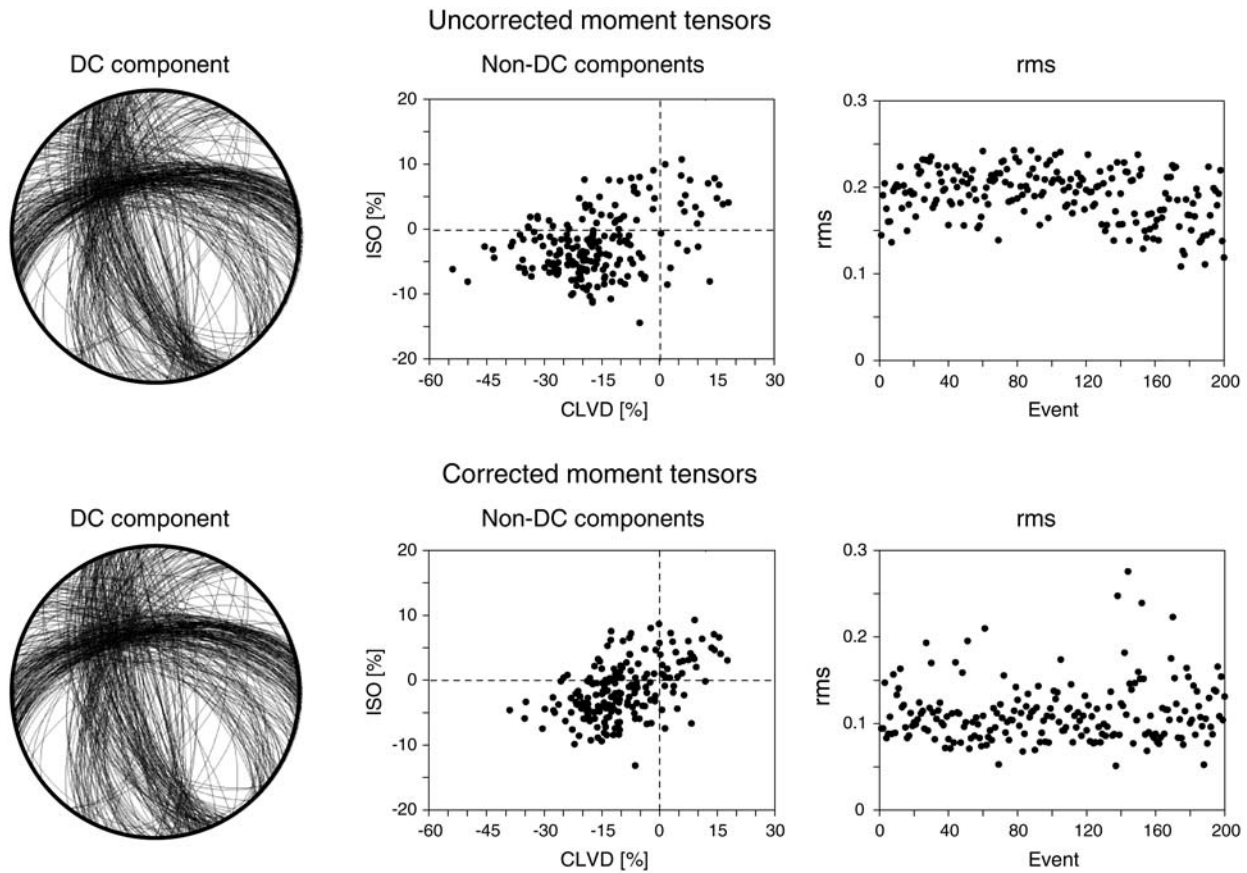


**Figure 15.** The moment tensors of 200 selected micro-earthquakes in West Bohemia retrieved using the uncalibrated (upper plots) and calibrated (lower plots) WEBNET network. The corrected moment tensors display low root-mean-square (rms) values and the non-double-couple (non-DC) components form a more compact cluster (for values, see Table 3). Also, the compensated linear vector dipole (CLVD) and isotropic (ISO) components have less pronounced negative values.

#### Moment Tensors Retrieved using the Calibrated Network

Finally, the moment tensors of the 200 selected events were calculated from the vertical  $P$ -wave amplitudes of the uncalibrated network (uncorrected moment tensors) and of the calibrated network (corrected moment tensors). The overall patterns of the focal mechanisms are almost indistinguishable for corrected and uncorrected moment tensors (Fig. 15, left-hand plots). This confirms the fact that the DC part of the moment tensors is rather stable. However, the non-DC components for corrected and uncorrected moment tensors differ (Fig. 15, middle plots). The non-DC components form a more compact cluster, and the CLVD and ISO components are less compressive (i.e., having less-pronounced negative values) for the corrected than for the uncorrected moment tensors. For example, the average value of the CLVD changed from  $-16.3\%$  for the original moment tensors to  $-9.7\%$  for the corrected moment tensors (see Table 3). The same tendency was observed also in the numerical modeling. The average value of the rms calculated in the moment-tensor inversion of the selected events is reduced from 0.19 to 0.11 (Table 3).

#### Discussion and Conclusions

In this paper, we propose a method for calibrating seismic networks in order to retrieve accurate moment tensors. The method is based on the joint inversion of large datasets of earthquakes for moment tensors and for network station amplifications, which encompass the instrumental amplifications of sensors, and the gain factor of the acquisition system, as well as the local site effects. The inversion works better for dense networks with good focal sphere coverage, for a high variety of focal mechanisms, and for large datasets of studied earthquakes. The method is capable of detecting reverse polarities, incorrect orientation and amplification of sensors and anomalous local site effects at stations. The inversion has been numerically tested for its accuracy and stability. The tests show that the moment tensors can be retrieved with higher accuracy after calibrating the network and properly correcting the observed amplitudes at stations.

The proposed inversion was applied to calibrating the WEBNET network of 22 local seismic stations using a dataset of 200 micro-earthquakes that occurred in 2008 in the West Bohemia region. The network calibration confirmed that all stations are of a correct polarity. However, station

amplification corrections display a rather high scatter of values ranging from 0.62 to 1.45 with the exception of station TRC the amplification correction of which is as much as 1.90. The high scatter in amplification corrections was not expected, and it can be attributed to a combination of local site effects and the inhomogeneity of the network equipped with a variety of different types of sensors at the individual stations. The accuracy of the retrieved amplifications is high, being about 2%–3% with an exception of KAC (6.0%) and HRED (5.6%). The KAC station has an unfavorable position on the focal sphere situated at the cross of the nodal lines of the analyzed focal mechanisms. The HRED station is rather noisy in comparison with the other stations.

The moment tensors retrieved using amplitudes of properly calibrated stations of the WEBNET network display lower rms than the original moment tensors. The reduction of the average rms was from 0.19 to 0.11. The focal mechanisms are not visibly changed by the calibration but the non-DC components of the moment tensors changed noticeably. This indicates that one of the origins of the spurious non-DC components might be linked to inaccurate station amplifications of seismic networks.

Finally, we would like to emphasize that the method is particularly suitable for applying to data gathered (1) in laboratory experiments; (2) in boreholes or in mines, where the calibration and orientation of the sensors are frequently unknown; or (3) in field experiments where the networks are inhomogeneous and consist of stations equipped with sensors of various types. Moreover, the method is capable to quantify and include into the moment tensor inversion the site effects and other effects of wave propagation neglected in the Green's functions. Therefore, the application of the method is desirable in all studies that intend to retrieve and interpret highly accurate moment tensors and, particularly, their non-DC components. If high-quality broadband observations are available, then a proper inversion performed in several frequency bands should even yield frequency dependent station amplifications.

## Data and Resources

All data used in this paper came from published sources listed in the references.

## Acknowledgments

We thank Alena Boušková, Josef Horálek, Tomáš Fischer, and other colleagues of the WEBNET group for providing us with the data from the 2008 swarm activity and for their kind help with data pre-processing, and Fateh Bouchaala for providing us with the accurate locations of the earthquakes under study. The detailed comments of Cezar Trifu and two anonymous reviewers are greatly appreciated. The work was supported by the Grant Agency of the Academy of Sciences of the Czech Republic, Grant IAA300120801; by the Grant Agency of the Czech Republic, Grant P210/12/1491; by the European Community's FP7 Consortium Project AIM (Advanced Industrial Microseismic Monitoring), Grant Agreement 230669; and by the project of large research infrastructure CzechGeo, Grant LM2010008.

## References

- Babuška, V., J. Plomerová, and T. Fischer (2007). Intraplate seismicity in the western Bohemian Massif (central Europe): A possible correlation with a paleo-plate junction, *J. Geodyn.* **44**, nos. 3–5, 149–159, doi: [10.1016/j.jog.2007.02.004](https://doi.org/10.1016/j.jog.2007.02.004).
- Červený, V. (2001). *Seismic Ray Theory*, Cambridge University Press, Cambridge.
- Cesca, S., E. Buforn, and T. Dahm (2006). Amplitude spectra moment tensor inversion of shallow earthquakes in Spain, *Geophys. J. Int.* **166**, no. 2, 839–854, doi: [10.1111/j.1365-246X.2006.03073.x](https://doi.org/10.1111/j.1365-246X.2006.03073.x).
- Davi, R., G. S. O'Brien, I. Lokmer, C. J. Bean, P. Lesage, and M. M. Mora (2010). Moment tensor inversion of explosive long period events recorded on Arenal volcano, Costa Rica, constrained by synthetic tests, *J. Volcan. Geotherm. Res.* **194**, no. 4, 189–200, doi: [10.1016/j.jvolgeores.2010.05.012](https://doi.org/10.1016/j.jvolgeores.2010.05.012).
- De Barros, L., I. Lokmer, C. J. Bean, G. S. O'Brien, G. Saccorotti, J. P. Metaxian, L. Zuccarello, and D. Patane (2011). Source mechanism of long period events recorded by a high density seismic network during the 2008 eruption on Mt. Etna, *J. Geophys. Res.* **116**, no. B01304, doi: [10.1029/2010JB007629](https://doi.org/10.1029/2010JB007629).
- Dziewonski, A. M., T. A. Chou, and J. H. Woodhouse (1981). Determination of earthquake source parameter from waveform data for studies of regional and global seismicity, *J. Geophys. Res.* **86**, no. B4, 2825–2852.
- Fischer, T., and J. Horálek (2003). Space-time distribution of earthquake swarms in the principal focal zone of the NW Bohemia/Vogtland seismoactive region: Period 1985–2001, *J. Geodyn.* **35**, nos. 1–2, 125–144, doi: [10.1016/S0264-3707\(02\)00058-3](https://doi.org/10.1016/S0264-3707(02)00058-3).
- Fischer, T., J. Horálek, J. Michálek, and A. Boušková (2010). The 2008 West Bohemia earthquake swarm in the light of the WEBNET network, *J. Seismol.* **14**, no. 4, 665–682, doi: [10.1007/s10950-010-9189-4](https://doi.org/10.1007/s10950-010-9189-4).
- Ford, S. R., D. S. Dreger, and W. R. Walter (2010). Network sensitivity solution for regional moment-tensor inversions, *Bull. Seismol. Soc. Am.* **100**, no. 5A, 1962–1970.
- Heidbach, O., M. Tingay, A. Barth, J. Reinecker, D. Kurfeß, and B. Müller (2008). The World Stress Map database release 2008, available using [www.world-stress-map.org/](http://www.world-stress-map.org/), doi: [10.1594/GFZ.WSM.Rel2008](https://doi.org/10.1594/GFZ.WSM.Rel2008) (last accessed February 2012).
- Julian, B. R., A. D. Miller, and G. R. Foulger (1997). Non-double-couple earthquake mechanisms at the Hengill-Grensdalur volcanic complex, southwest Iceland, *Geophys. Res. Lett.* **24**, no. 2, 743–746.
- Lay, T., and T. C. Wallace (1995). *Modern Global Seismology*, Academic Press, San Diego.
- Müller, B., M. L. Zoback, K. Fuchs, L. Mastin, S. Gregersen, N. Pavoni, O. Stephansson, and C. Ljunggren (1992). Regional patterns of tectonic stress in Europe, *J. Geophys. Res.* **97**, no. B8, 11,783–11,803, doi: [10.1029/91JB01096](https://doi.org/10.1029/91JB01096).
- Šílený, J., and R. Hofstetter (2002). Moment tensor of the 1999 Dead Sea calibration shot: Limitations in the isotropic source retrieval without a detailed earth model, *Tectonophysics* **356**, nos. 1–3, 157–169, doi: [10.1016/S0040-1951\(02\)00382-7](https://doi.org/10.1016/S0040-1951(02)00382-7).
- Sipkin, S. A. (1986). Estimation of earthquake source parameters by the inversion of waveform data: Global seismicity, 1981–1983, *Bull. Seismol. Soc. Am.* **76**, no. 6, 1515–1541.
- Trifu, C.-I., and V. Shumila (2000). The use of uniaxial recordings in moment tensor inversions for induced seismic sources, *Tectonophysics* **356**, nos. 1–3, 171–180, doi: [10.1016/S0040-1951\(02\)00383-9](https://doi.org/10.1016/S0040-1951(02)00383-9).
- Vavryčuk, V. (2001). Inversion for parameters of tensile earthquakes, *J. Geophys. Res.* **106**, no. B8, 16,339–16,355, doi: [10.1029/2001JB000372](https://doi.org/10.1029/2001JB000372).
- Vavryčuk, V. (2002). Non-double-couple earthquakes of January 1997 in West Bohemia, Czech Republic: Evidence of tensile faulting, *Geophys. J. Int.* **149**, no. 2, 364–373, doi: [10.1046/j.1365-246X.2002.01654.x](https://doi.org/10.1046/j.1365-246X.2002.01654.x).
- Vavryčuk, V. (2007). On the retrieval of moment tensors from borehole data, *Geophys. Prospect.* **55**, no. 3, 381–391, doi: [10.1111/j.1365-2478.2007.00624.x](https://doi.org/10.1111/j.1365-2478.2007.00624.x).

- Vavryčuk, V. (2011a). Principal earthquakes: Theory and observations for the 2008 West Bohemia swarm, *Earth Planet. Sci. Lett.* **305**, nos. 3–4, 290–296, doi: [10.1016/j.epsl.2011.03.002](https://doi.org/10.1016/j.epsl.2011.03.002).
- Vavryčuk, V. (2011b). Detection of high-frequency tensile vibrations of a fault during shear rupturing: Observations from the 2008 West Bohemia swarm, *Geophys. J. Int.* **186**, no. 3, 1404–1414, doi: [10.1111/j.1365-246X.2011.05122.x](https://doi.org/10.1111/j.1365-246X.2011.05122.x).
- Vavryčuk, V. (2011c). Tensile earthquakes: Theory, modeling, and inversion, *J. Geophys. Res.* **116**, no. B12320, doi: [10.1029/2011JB008770](https://doi.org/10.1029/2011JB008770).
- Zahradník, J., J. Janský, and V. Plicka (2008a). Detailed waveform inversion for moment tensors of  $M$  4 events: Examples from the Corinth Gulf, Greece, *Bull. Seismol. Soc. Am.* **98**, no. 6, 2756–2771, doi: [10.1785/0120080124](https://doi.org/10.1785/0120080124).
- Zahradník, J., E. Sokos, G. A. Tselentis, and N. Martakis (2008b). Non-double-couple mechanism of moderate earthquakes near Zakynthos, Greece, April 2006; explanation in terms of complexity, *Geophys. Prospect.* **56**, no. 3, 341–356, doi: [10.1111/j.1365-2478.2007.00671.x](https://doi.org/10.1111/j.1365-2478.2007.00671.x).

Institute of Geophysics, Academy of Sciences  
Boční II/1401  
141 00 Praha 4  
Czech Republic

Manuscript received 16 December 2011